Measurement of the static friction coefficient in an Automatic Balancing Unit with dry friction

Measurement of the static friction coefficient in an Automatic Balancing Unit with dry friction

H.M.R. Suy

Report No. DCT 2003-22

Internship Committee:
Prof. dr. H. Nijmeijer (chairman)
Dr. ir. N. van de Wouw (coach)
Ir. R.A. van Rooij

Eindhoven University of Technology
Department of Mechanical Engineering
Dynamics and Control Group

Eindhoven, 6th May 2003

Abstract

Imbalance is encountered in many rotating systems. A possible solution in the reduction of unwanted effects of imbalance, such as vibrations, noise and increased wear, is an Automatic Balancing Unit (abbreviated ABU). An ABU is an example of a ball balancer where a number of freely moving balls position themselves in such a way that they counteract the imbalance. In contrast to most ball balancers, the usage of the ABU in optical systems like CD-ROM players prohibits the application of lubricants. The balls move towards isolated equilibrium *points* when a lubricant is applied. Without lubricant, dry friction causes the equilibria to become *sets* of ball positions. The static friction coefficient influences the size of these sets.

Subject of this research is the design and conduction of a friction measurement in order to identify the static friction level in an ABU. Hereto, a dynamic model of an ABU, containing one ball and rigidly attached to the world, is derived using Lagrange's equations of motion for systems with constraints. A set-valued Coulomb friction model is used to represent the stiction behaviour of the ball and is integrated in the ABU model. This model is numerically implemented in MATLAB and simulations are performed. The experimental setup imposes some restrictions regarding the control of the ABU and the reference trajectory of the rotational velocity of the ABU. The control law of the experimental setup is identified and implemented in the ABU model. Simulations of the model with control law show that only a confidence interval on the static friction coefficient can be found. With the aid of these simulations, a reference trajectory is designed for the use in experiments.

Using high-speed camera images, measurements on an experimental setup (partially provided by Philips Optical Storage) offer information on the angular position of the ball and ABU. While the lighting of the setup proves to have large influence on the image-processing and measurement results, various lighting-setups are tested. With the eventually obtained experimental setup a number of experiments are performed, resulting in a confidence interval on the static friction coefficient. An error analysis is performed to investigate the inaccuracy of the bounds of this interval.

Samenvatting

Roterende systemen zijn vaak onderhevig aan een zekere mate van onbalans. Een mogelijke oplossing in het reduceren van ongewenste effecten, veroorzaakt door een dergelijke onbalans, zoals trillingen, lawaai en verhoogde slijtage, is een Automatic Balancing Unit (afgekort ABU). Een ABU is een voorbeeld van een kogel-balanceerder waarin een aantal vrij bewegende kogels zichzelf ten opzichte van de onbalans zodanig positioneren dat deze (deels) gecompenseerd wordt. In tegenstelling tot de meeste kogel-balanceerders, kunnen in de ABU, vanwege het gebruik ervan in optische systemen zoals CD-ROM spelers, geen smeermiddelen worden toegepast. Wanneer een smeermiddel wordt gebruikt, bewegen de kogels zich richting geïsoleerde *evenwichtspunten*. Zonder smeermiddel zorgt droge wrijving ervoor dat het evenwicht zich uitstrekt naar *gebieden* van kogel posities. De statische wrijvingscoëfficiënt beïnvloedt de grootte van deze gebieden.

Onderwerp van dit onderzoek is het ontwerpen en uitvoeren van een wrijvingsmeting met het oog op het identificeren van het statische wrijvingsniveau van een ABU. Hiertoe is een dynamisch model van een ABU, één kogel bevattend en star aan de wereld bevestigd, afgeleid met behulp van de methode van Lagrange voor systemen met constraints. Een Coulomb wrijvingsmodel is gebruikt om het stick-gedrag van de kogels te representeren en is geïntegreerd in het ABU model. Dit model is numeriek geïmplementeerd in MATLAB en simulaties zijn uitgevoerd. De experimentele opstelling biedt enige beperkingen op het gebied van de regeling van de ABU en de trajectorie die als referentie van de hoeksnelheid van de ABU kan worden opgegeven. De regelwet van de experimentele opstelling is geïdentificeerd en geïmplementeer in het ABU model. Uit simulaties van het model met regelwet blijkt dat slechts een betrouwbaarheidsinterval van de statische wrijvingscoëfficiënt kan worden bepaald. Met behulp van deze simulaties is een referentie trajectorie ontworpen die kan worden toegepast tijdens experimenten.

Metingen aan een experimentele opstelling (deels ter beschikking gesteld door Philips Optical Storage) met een high-speed camera, leveren gegevens betreffende de hoekpositie van zowel de kogel als de ABU. Omdat de belichting van de opstelling een grote invloed blijkt te hebben op de beeldverwerking en de meetresultaten, zijn verschillende belichtingsopstellingen uitgeprobeerd. Vervolgens zijn een aantal metingen aan de uiteindelijk verkregen experimentele opstelling verricht. Hieruit volgt een betrouwbaarheidsinterval van de statische wrijvingscoëfficiënt. Een foutenanalyse is uitgevoerd om de onnauwkeurigheid van de grenzen van dit interval te bepalen.

Contents

Chapter 1

Introduction

1.1 Working principle of the ABU

Many rotating systems exhibit imbalances. The magnitude or position of these imbalances can often not be determined or varies during the operation cycle of the system. In these cases, the imbalance can not be compensated for in the design of the system. The resulting vibrations can cause unwanted effects such as noise, increased wear or deteriorated performance of the system. Elimination or reduction of these effects can be accomplished by, for instance, an Automatic Balancing Unit (abbreviated ABU). This possible solution is subject of this research.

The ABU is designed by Philips Optical Storage (POS) for the use in CD-ROM players. In most cases, ball-balancers (such as the ABU) are used with a lubricant. This reduces (or eliminates) the friction in the contact surface between ball and ABU. Because of the use of this balancer in optical systems, application of lubricants is not possible.

In figure 1.1 a picture of the ABU is shown. It is composed of a circular polycarbonate disk with upright rim in which a number of balls are placed. In this study brass balls are used. The balls can move freely in the disk and are propelled outwards by the rotation of the ABU around its geometrical center, pushing them onto the rim. The balls move on the surface of the rim under influence of dry friction while no lubricant is used. In the rim a very small groove is present in which the balls rotate. The curvature of this groove is chosen in such a way that the balls (theoretically) have a point-contact with the rim.

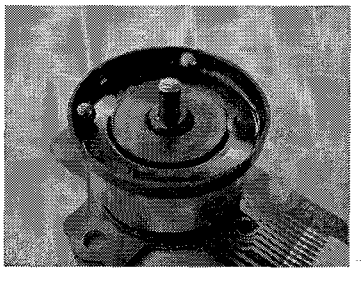

Figure 1.1: Picture of the Automatic Balancing Unit mounted on a motor.

When the motor with ABU is rotated, imbalances in for instance the CD (not shown in figure 1.1) cause vibrations. These vibrations make the balls move towards equilibrium positions. Below the systems eigenfrequency, the equilibrium positions are located at the side of the imbalance, thus amplifying the vibration. However, the equilibria above the eigenfrequency are positioned

opposite to the imbalance [1]. This balancing action of the ABU reduces the vibration of the system relatively to the fixed world.

1.2 Introduction to the friction model

Because the balls in the ABU show stick behaviour, the friction is modelled using a set-valued or Coulomb friction model (see figure 1.2). To avoid confusion, some terminology that will be used throughout this report, will be introduced in this section.

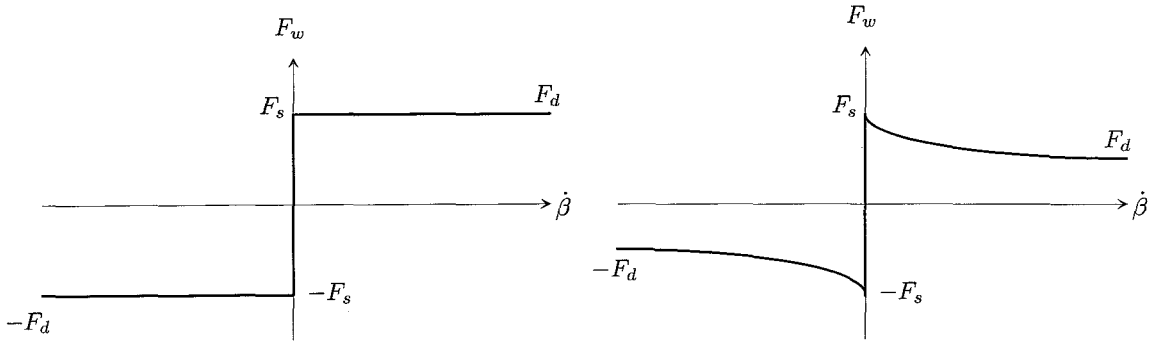

Figure 1.2: Coulomb friction without (left) and with (right) Stribeck effect.

- *Relative velocity, slip and stick:* The angular position of a ball relatively to the ABU is called β. Because the ball is assumed to perform a purely rolling motion, the relative velocity in the contacting surfaces of ball and ABU is always equal to zero. When the ball is, however, rolling on the surface of the ABU, the relative angular velocity ($\dot{\beta}$) is unequal to zero. The ball is then said to be in *slip* with nonzero relative velocity, although no slip occurs in the contacting surfaces. On the other hand, the term *stick* is used when the ball is not rolling.

- *Static friction level or force:* Maximum absolute value of the frictional force F_w for which no relative movement between ball and ABU is eminent (e.g. $\dot{\beta} = 0$). In figure 1.2, the static friction level is denoted by F_s and $-F_s$.

- *Dynamic friction level or force:* Value of the frictional force F_w in case of relative movement (e.g. $\dot{\beta} \neq 0$), denoted by $\pm F_d$ in figure 1.2. For the sake of simplicity, the dynamic friction level in this research is chosen equal to the static one, in accordance with the left part of figure 1.2.

- *Static friction coefficient:* Quotient between the static friction force and the normal force acting on a ball, denoted by the symbol μ [-].

- *Set-valued model:* For $\dot{\beta} = 0$ the friction force F_w is described by a set-valued function, counteracting the resultant force of all other external forces that act on the ball. This friction force is bounded by the static friction level, so $F_w \in [-F_s \quad F_s]$.

As a final remark, one other phase besides slip and stick is introduced. This *transition* phase is characterized by $\dot{\beta} = 0$ and $\ddot{\beta} \neq 0$ and plays an important role in the numerical implementation of the model in MATLAB. Moreover, a Switch Model is used in the numerical implementation. A description of this Switch Model is given in [2] and [1].

1.3 Motivation of the project and problem formulation

When no dry friction is apparent (by using for instance a lubricant), the resulting equilibria mentioned in section 1.1 are isolated points. In the case of the ABU, dry friction causes the equilibria to become sets of ball configurations [1]. The magnitude of the static friction level directly influences the size of these sets. The dynamic friction level can affect the stability of the equilibrium sets.

In previous research ([1], [3]), experiments were performed to determine the static friction level. In [1], the static friction level was determined by using the deceleration profile of a ball when the ABU was slowed down from a certain rotational velocity to a standstill instantaneously. Only one ball was used to avoid collisions and friction between balls. This dynamical friction was then assumed to be equal to the static friction level. Because of the poor results of this test, the static friction coefficient was determined in such a way that simulation results of a derived ABU-model matched experimental ones. Validation showed, however, that the obtained value could not account for all the experimental results.

In [3], the static friction coefficient was determined using an experiment performed outside the ABU. Three balls were placed between two plates of the same polycarbonate material as used for the ABU and into straight parallel grooves with identical dimensions as the ones in the ABU. By placing these two plates onto a tilting-device, the angle at which the upper plate started sliding was measured. This angle was adjusted using a spindle and relates to the static friction level. The resulting value of μ had the same order of magnitude as in [1]. Remarks could be made on the correctness of this measurement. The normal forces acting on the balls induced by the upper plate were much larger than the ones experienced by the balls in the ABU. Furthermore, it is likely that rotation of the spindle and tilting of the plates introduced vibrations to the experimental setup, causing the upper plate to slip even before the static friction level was reached. Because the obtained static friction value could also not account for all experimental results in [1], the demand arose to design a new experiment to measure the static friction force more accurately.

This leads to the following problem formulation for this study:
Design and perform a friction measurement on an Automatic Balancing Unit with dry friction in order to identify the static friction level.

1.4 Outline of the report

Chapter 2 begins with the elaboration of the general idea behind the static friction coefficient measurement. Hereto, an example of a block on an accelerating underground is regarded. Chapter 3 discusses the adaptation of this friction measurement idea to the ABU. This will be done by first elucidating the kinematics of a model of an ABU that is fixed to the world with one ball inside of it. Next, the dynamical modelling will be considered.

Simulations, both with explicitly prescribed ABU motion and with practical limitations from the experimental setup, will be discussed in chapter 4. The limitations from the latter type of simulations are mainly caused by the ABU controller and the reference trajectory of the rotational velocity of the ABU. In order to perform such simulations, a control law is identified and implemented in the ABU model. From these simulations, a reference signal results that can be used in experiments. The experiments and eventually obtained measurement results are found in chapter 5. Moreover, an error analysis and discussion of the results will be presented in this chapter. Finally, conclusions and recommendations will be given in chapter 6.

Chapter 2

Idea behind the static friction level measurement

2.1 Friction measurement of a block gliding on an underground

As already mentioned in chapter 1, the stiction behaviour of the ball(s) inside the ABU is modelled using a Coulomb friction model. This model can also be used to characterize the dry friction between two surfaces gliding relatively over each other. In the following example of a block on an underground it will become clear how the static friction level can be calculated from a given velocity profile of the underground.

The only force acting in the direction of movement on a block resting on an underground is the friction force F_w (see figure 2.1). This force acts like a constraint force; it tries to give the block the same acceleration as the underground. It is, however, bounded by its static friction

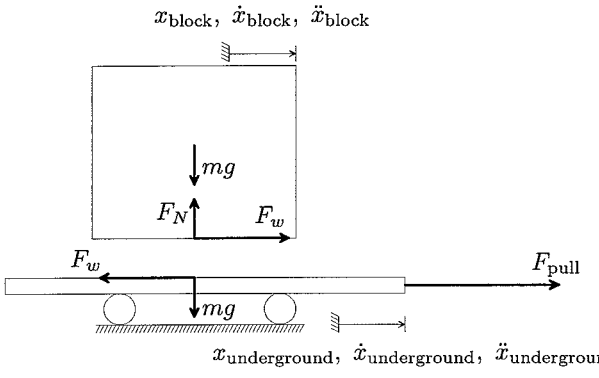

Figure 2.1: Forces acting on a block resting on an acceleration underground.

level. This level determines the maximum value of the acceleration of the underground that can be 'followed' by the block. The force needed to accelerate the block can be easily calculated using $F_w = m\,a$ with m the mass of the block [kg] and a the acceleration [m/s^2]. As long as this force is less than or equal to the static friction level, the block will accelerate with the same magnitude as the underground. When this is not the case, the acceleration of the block will remain constant while F_w has reached its constant maximum value, whereas the acceleration of the underground can attain a higher value, inducing slip in the contacting surface. Here, the assumption is made

that the Coulomb friction model without Stribeck effect is used.

To measure the static friction force, it suffices to measure the acceleration a_{slip} at the exact moment when slip occurs (this time-instant will be called the slip-point). The static friction force can be easily calculated using the following equation:

$$F_s = m\, a_{\text{slip}}\,. \tag{2.1}$$

The static friction coefficient is then equal to:

$$\mu = \frac{F_s}{F_N}\,, \tag{2.2}$$

with the normal force $F_N = mg$ and g the gravitational acceleration [m/s^2].

This static friction level measurement method is implemented and tested in MATLAB. By applying a linearly increasing acceleration profile on the underground (and thus a quadratic velocity profile), the slip-point can be identified easily. For a certain value of μ and m the resulting velocities of both underground and block are given in figure 2.2. The slip-point is detected when the relative velocity between block and underground surpasses a certain small tolerance.

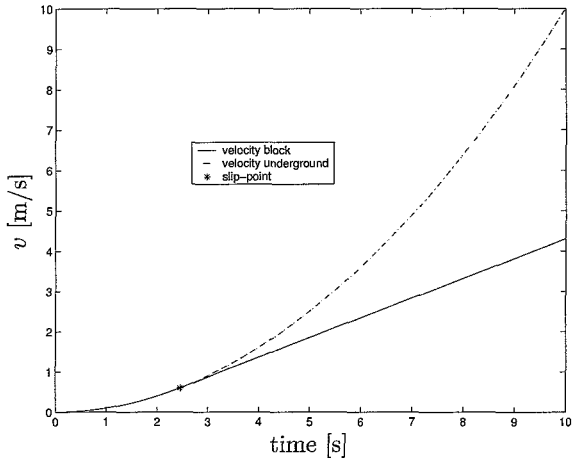

Figure 2.2: Velocity of a block with mass m on an accelerating underground with dry friction.

Chapter 3

Dynamic model of the ABU

3.1 Model definition

To be able to apply the static friction level measurement, discussed in chapter 2, to the ABU system, a dynamic model is derived. In figure 3.1, the model of the ABU is shown. The ABU system consists of a table on which a motor is attached. The circular disk of the ABU is mounted onto the rotor part of the motor by means of a tight fitting. Moreover, a CD is glued to this part of the motor. The geometrical center of the ABU is located at point B. The whole table is rigidly

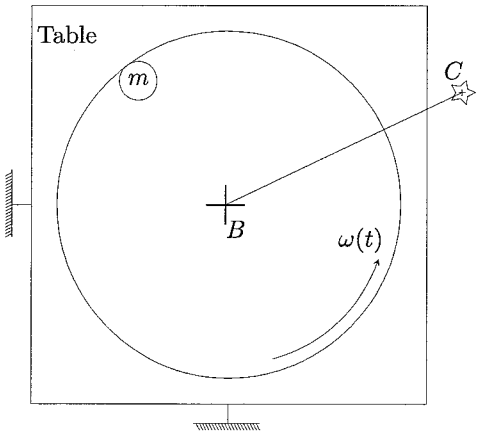

Figure 3.1: Model definition of the ABU.

attached to the inertial space or fixed world (in the experimental setup this is a granite block of considerable mass) by two clamps. All degrees of freedom of the ABU, apart from the rotational one around its geometrical center, are fixed. Because this eliminates the vibration of the ABU relatively to the world, all ball positions are equilibria. The rotational velocity of the ABU around point B is called $\omega(t)$. To avoid collisions and friction between balls, only one ball is used. This ball, with mass m, can move freely in the ABU, but is assumed to be always in contact with the rim and to perform a purely rolling motion. To be able to define the angular position of the ball relatively to the ABU, a marker is positioned on the CD, represented by point C. Furthermore, all movements are assumed to take place in the horizontal plane.

3.2 Kinematics of the ABU model

Figure 3.2 shows the kinematics, the used coordinate systems and generalized coordinates. Coordinate system ($\vec{e}_1$,$\vec{e}_2$) represents inertial space and has its origin in point B, while flexibility between rotor and stator part of the motor is neglected. The same point is used as the origin of coordinate system ($\vec{e}_x$,$\vec{e}_y$), where the vector $\vec{e}_x$ is pointing from point B to C. Its movement can be

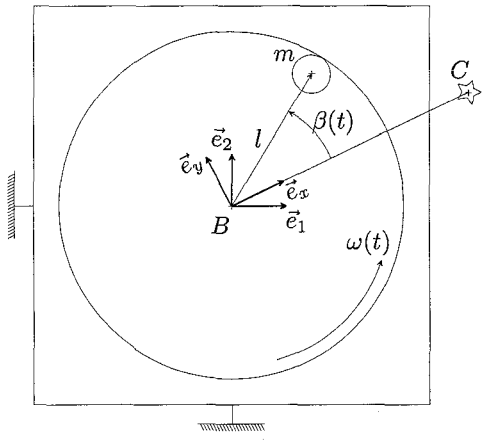

Figure 3.2: Kinematics of the ABU model.

prescribed by the angular rotation with velocity $\omega(t)$. The relationship between both right-handed coordinate systems is given by:

$$\begin{bmatrix}\vec{e}_x\\ \vec{e}_y\end{bmatrix} = \begin{bmatrix}\cos\theta(t) & \sin\theta(t)\\ -\sin\theta(t) & \cos\theta(t)\end{bmatrix}\begin{bmatrix}\vec{e}_1\\ \vec{e}_2\end{bmatrix}, \tag{3.1}$$

where $\theta(t)$ is defined as $\theta(t) = \int_0^t \omega(\tau)d\tau$, with $\theta(0) = 0$. The position of the ball is defined by l and $\beta(t)$. Here l determines the distance from point B to the center of gravity of the ball and $\beta(t)$ the angle $\angle CBm$. The position vector $\vec{r}_{A_m}$ is given by:

$$\vec{r}_{A_m} = \begin{bmatrix}l\cos\beta & l\sin\beta\end{bmatrix}\begin{bmatrix}\vec{e}_x\\ \vec{e}_y\end{bmatrix}. \tag{3.2}$$

Here, the dependency of β on time t is omitted. This will also be done for all other time-dependent coordinates throughout the rest of the report. The system can thus be described by the column of generalized coordinated $\underline{q} = \begin{bmatrix}\beta & l\end{bmatrix}^T$. The choice for these two coordinates will be explained in section 3.3.

3.3 Dynamic modelling of the ABU

The dynamic model of the ABU is derived using Lagrange's Method [4]. This section will provide the resulting equations of motions. The complete derivation can be found in appendix A.

The normal force acting on a ball can be regarded as a constraint force, enforcing that the ball is always in contact with the rim of the ABU. Although this implies that l is constant, it is used as a generalized coordinate to enable calculation of this force [1]. Hereto Lagrange's Equations of Motion are expanded into *Lagrange's Equations for systems with constraints* [4]:

$$\frac{d}{dt}(T_{,\underline{\dot{q}}}) - T_{,\underline{q}} + V_{,\underline{q}} = (\underline{Q}^{\mathrm{nc}})^T + (\underline{R}^T\underline{\lambda})^T, \tag{3.3}$$

with:

$\underline{q}$	column of generalized coordinates, $\underline{q} = [\beta \quad l]^T$;
T	kinetic energy;
V	potential energy;
$\underline{Q}^{\text{nc}}$	column with generalized non-conservative forces;
$\underline{R}^T\underline{\lambda}$	column of generalized constraint forces.

The constraint equations are written at acceleration level, resulting in the following relationship between $\underline{R}$ and $\ddot{\underline{q}}$:

$$\underline{R}\ddot{\underline{q}} = \underline{0}\,. \tag{3.4}$$

Equation (3.3) leads to:

$$\underline{M}(\underline{q})\ddot{\underline{q}} - \underline{h}(\underline{q},\dot{\underline{q}}) = \underline{R}^T\underline{\lambda}, \tag{3.5}$$

where the frictional forces are included in the column $\underline{h}(\underline{q},\dot{\underline{q}})$. The Coulomb friction model states that there is a dependency of the friction force on the normal force: $F_w \in \mu F_N \text{Sign}(\dot{\beta})$. Herein, Sign is a set-valued function as described in section 1.2. Depending on the state of the ball (i.e. *Slip*, *Stick* or *Transition*), the frictional force is either proportional to F_N or a constraint function itself, counteracting all other external forces that work on the ball. Because $\underline{h}(\underline{q},\dot{\underline{q}})$ is not allowed to be a function of the constraint forces, the following reformulation of (3.5) is applied:

$$\underline{M}(\underline{q})\ddot{\underline{q}} - \underline{h}(\underline{q},\dot{\underline{q}}) + \underline{S}\,\underline{\lambda} = \underline{R}^T\underline{\lambda}\,. \tag{3.6}$$

Clearly, the dimension of both $\underline{S}$ and $\underline{R}$ depend on the state of the ball. For all possible configurations, the expressions for $\underline{S}$, $\underline{R}$ and $\underline{\lambda}$ are given in appendix A.6. In this section, the results for $\underline{M}(\underline{q})$ and $\underline{h}(\underline{q},\dot{\underline{q}})$ will be given:

$$\underline{M}(\underline{q}) = \begin{bmatrix} ml^2 + J(\frac{2l}{d})^2 & 0 \\ 0 & m \end{bmatrix}, \tag{3.7}$$

$$\underline{h}(\underline{q},\dot{\underline{q}}) = \begin{bmatrix} h_\beta & h_l \end{bmatrix}^T, \tag{3.8}$$

with:

$$\begin{aligned} h_\beta &= -\{ml^2 - J(\tfrac{2l}{d})\}\ddot{\theta}\,, \\ h_l &= -\{J\tfrac{2}{d}\dot{\theta}\dot{\beta} - ml(\dot{\beta}+\dot{\theta})^2 - J(\tfrac{4l}{d^2})\dot{\beta}^2\}\,. \end{aligned}$$

The symbol J is used to denote the mass moment of inertia of the ball with respect to its center of gravity ($J = \frac{1}{10}md^2$ [kg m^2]) where d represents the diameter of the ball [m]. The parameter values equal [1]:

$$\begin{aligned} m &= 1.4 \cdot 10^{-4} \text{ kg}\,, \\ d &= 3.0 \cdot 10^{-3} \text{ m}\,, \\ l &= 1.15 \cdot 10^{-2} \text{ m}\,. \end{aligned}$$

Combination of (3.4) and (3.6) enables calculation of the constraint forces and accelerations of the generalized coordinates:

$$\underline{\lambda} = -[\underline{R}\,\underline{M}(\underline{q})^{-1}(\underline{R}^T - \underline{S})]^{-1}\underline{R}\,\underline{M}(\underline{q})^{-1}\underline{h}(\underline{q},\dot{\underline{q}})\,, \tag{3.10}$$

$$\ddot{\underline{q}} = \underline{M}(\underline{q})^{-1}\{\underline{h}(\underline{q},\dot{\underline{q}}) + (\underline{R}^T - \underline{S})\underline{\lambda}\}\,. \tag{3.11}$$

Because the constraint equations are written at acceleration level, small numerical errors may cause the term $\underline{R}\ddot{q}$ in (3.4) to be not equal to zero. Integration of this term in time causes numerical drift of the actual constraint. To avoid this, constraint stabilization should be applied. In this research, $\ddot{l}$ is explicitly set to zero at each iteration. Furthermore, as already mentioned in chapter 1, the Switch Model is used. For a more detailed description on this subject and the numerical implementation of the equations of motion in MATLAB the reader is referred to [1].

Chapter 4

Simulations on the ABU model

4.1 Static friction coefficient measurement with prescribed ABU motion

As in chapter 2, static friction level measurement in the ABU translates into finding the (angular) acceleration of the ABU at the time when the ball starts rolling. To derive more insight in this procedure, simulations are conducted in MATLAB. Although not applicable to the experimental setup, first some simulations are performed in which the angular acceleration, velocity and position profile of the ABU are prescribed explicitly. This is done for the sake of simplicity. Moreover, this offers good possibilities to verify the derived dynamic ABU model. Simulations based on the restrictions of the practical setup will be discussed in section 4.2.

The initial rotational velocity of the ABU is chosen unequal to zero, simulating the ball to be in contact with the rim ($\dot{l} = 0$). Furthermore, the ABU is assumed to be held at that velocity long enough to assure the ball to be in stick-phase. On simulation level this is done by choosing the initial condition of the relative angular velocity between ball and ABU equal to zero (e.g. $\dot{\beta}(t = 0) = \dot{\beta}_0 = 0$). The initial relative angle β_0 is chosen arbitrarily.

As in the experimental setup, the ABU is simulated to rotate clockwise (in negative direction). For a linear rotational acceleration profile $\dot{\omega}$ and thus a quadratic rotational velocity profile with initial velocity $\omega_0 = -20$ Hz, the resulting β and $\dot{\beta}$ are shown in figures 4.1 and 4.2, respectively.

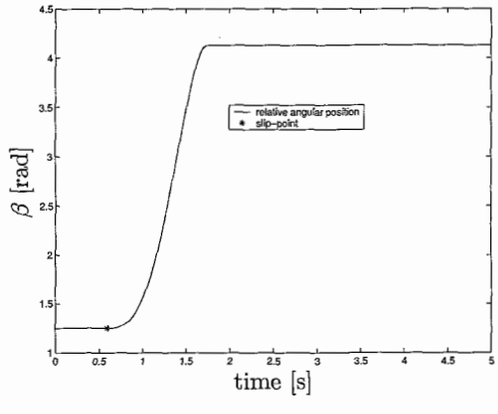

Figure 4.1: Relative angular position β between ball and ABU, $\beta_0 = 1.25$ rad.

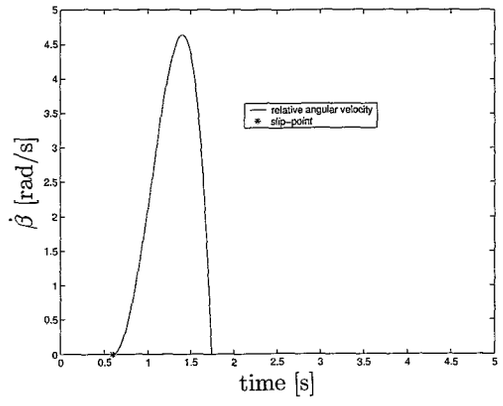

Figure 4.2: Relative angular velocity $\dot{\beta}$ between ball and ABU [rad/s].

At some point during the motion-profile of the ABU, slip occurs. The ball starts rolling but eventually comes to a rest at some position and remains there. This is caused by the fact that with the quadratic increasing of ω also the normal force acting on the ball increases according to $F_N = ml\omega^2$. With the Coulomb friction model and a static friction coefficient that does not depend on the normal force, the static friction force increases as well, until it is large enough to make the ball stick. Furthermore, while the ABU accelerates in negative direction, β moves in positive direction.

The slip-point is detected when $\dot{\beta}$ becomes larger than a tolerance ϵ of order 10^{-7} rad/s. When $\dot{\beta}$ and $\ddot{\beta}$ are assumed to be negligible small in the slip-point, the static friction force can be calculated using the equations of motion:

$$F_s = -\frac{\{ml^2 - \frac{2l}{d}J\}\dot{\omega}_{slip}}{l}. \tag{4.1}$$

Herein, $\dot{\omega}_{slip}$ is the value of the rotational acceleration of the ABU in the slip-point. An approximation of the static friction coefficient μ is then easily found by dividing the static frictional force through the value of the normal force in the slip-point ($F_N = ml\omega_{\text{slip}}^2$)[1]:

$$\mu = \frac{F_s}{F_N}. \tag{4.2}$$

4.2 Static friction coefficient measurement with practical restrictions

4.2.1 Identification and implementation of the ABU controller

At the experimental setup, the rotational velocity of the ABU is controlled using a PI-action on the error between the desired rotational velocity and the actual velocity; $e_\omega = \omega_{ref} - \omega$ [5]. It is assumed that the ABU can be described by a second order system without friction. The equation of motion equals:

$$J_{\text{ABU}}\,\ddot{\theta} = T, \tag{4.3}$$

[1] when accelerating the ABU in positive direction, the sign of $\dot{\beta}$ in the slip-point should also be taken into account while μ is positive and equals $\frac{F_w}{F_N \text{Sign}(\dot{\beta})}$

where J_{ABU} is the mass moment of inertia of the ABU around its center of mass and T the applied torque following from the PI-action on the angular velocity error:

$$T = K_p\, e_\omega + K_I \int_0^t e_\omega(\tau) d\tau\,. \tag{4.4}$$

Herein, K_p and K_I are parameters of the proportional and integrating action, respectively. While $\theta(t) = \int_0^t \omega(\tau) d\tau$, (4.4) yields the following differential equation in terms of θ:

$$\begin{aligned} J_{\text{ABU}}\,\ddot{\theta} + K_P\,\dot{\theta} + K_I\,\theta &= K_P\,\dot{\theta}_{ref} + K_I\,\theta_{ref}\,, \\ &\text{or,} \\ \ddot{\theta} + 2\xi\omega_n\,\dot{\theta} + \omega_n^2\,\theta &= 2\xi\omega_n\,\dot{\theta}_{ref} + \omega_n^2\,\theta_{ref}\,. \end{aligned} \tag{4.5}$$

The parameters ξ and ω_n are found by performing a short experiment. In this experiment, the ABU is subjected to a step reference and speeded up from zero velocity to a certain setpoint ω_{ref}. An optical sensor, attached to the fixed world and placed above the ABU, generates a pulse every time one side of a thread, spanned across the CD mounted on the motor, passes the sensor. From these pulses the rotational velocity ω is derived. The percentage of overshoot and settling-time in reaching the setpoint is used to identify ξ and ω_n. The obtained control parameters equal:

$$\begin{aligned} \xi &= 0.5\,, \\ \omega_n &= 2.2 \text{ rad/s}\,. \end{aligned}$$

It should be noted that the derived controller only approximates the actual controller. However, for the purpose of simulation, the found control action is very useful in designing a reference trajectory that can be used in experiments. This reference trajectory should be designed in such a way that slip occurs and that the slip-point can be used to calculate the static friction coefficient or a confidence interval of it.

The control law (4.5) is integrated into the equations of motion of the ABU. Hereto, the generalized coordinates are expanded with θ; $\underline{q} = \begin{bmatrix}\beta & l & \theta\end{bmatrix}^T$. The frictional torque applied by the ball on the ABU is disregarded after validation of this assumption.

4.2.2 Design of a reference trajectory

The controller of the experimental setup can only handle setpoints or series of setpoints placed in a profile [5]. The setpoint resolution in the practical setup is equal to 1 Hz, so no smooth reference trajectory can be applied. If a change of setpoint $\Delta\omega$ is given to the derived controller in (4.5) at time t_s, the rotational velocity ω starts to go to the new setpoint with a slope at time t_s unequal to zero. In other words, the rotational acceleration $\dot{\omega}$ changes discontinuously at t_s. Depending on the value of the static friction coefficient μ and the applied step $\Delta\omega$, the ball can start to roll *instantaneously* (at t_s). This is the case when the value of the friction force needed to keep the ball in stick while the system is excited with $\dot{\omega}(t_s)$, is larger than the static friction force.

Another implication of the discontinuous behaviour of $\dot{\omega}$ is the fact that it is impossible to find the exact value of $\dot{\omega}$ when slip occurs ($\dot{\omega}_{slip}$ in (4.1)). To be able to give a confidence interval on μ, it is therefore needed to be able to define an upper and lower-bound. Hereto, a reference trajectory of ω should be designed that results in a discontinuous signal $\dot{\omega}$, where at least one value of $\dot{\omega}$ (unequal to zero) should be found where the ball remains in stick and one value where the ball *instantly* starts to slip. It can then be stated that the actual value of the static friction coefficient μ must be between the values obtained with:

$$\begin{aligned} \mu_{\text{low/high}} &= \frac{\{ml^2 - \frac{2l}{d}J\}|\dot{\omega}_{\text{low/high}}|}{ml^2\omega^2_{\text{low/high}}}\,, \\ \mu_{\text{low}} &\leq \mu < \mu_{\text{high}}\,. \end{aligned} \tag{4.7}$$

Herein, the indices low and high denote the cases where the ball remains in stick or starts to slip, respectively. The absolute value of $\dot{\omega}$ is taken because of the influence of the sign of $\dot{\beta}$ as discussed in section 4.1.

Due to the fact that the smallest step size $\Delta\omega$ in the experimental setup is 1 Hz, the reference trajectory should become a sequence of steps. Slip is more likely to occur when μ is small, resulting in a lower static friction level for the same normal force, or when the initial rotational velocity ω_0 at the beginning of a step is small. The latter is caused by the fact that for small velocities the normal force on a ball is small as well, resulting in a lower static friction level. Because the first step in the trajectory is not allowed to make the ball slip (to be able to identify μ_{low}), it is studied what the value of ω_0 at the start of a step of 1 Hz should be, in order to keep the ball in stick-phase. Because this value depends on the static friction coefficient, μ is varied between the value found in [1] and a number of times this value. The results are shown in table 4.1. When the

Table 4.1: Value of ω_0 for different values of μ at which a step of 1 Hz does not cause slip.

μ [-]	ω_0 [Hz]
$2.75 \cdot 10^{-3}$	17
$2 \cdot 2.75 \cdot 10^{-3}$	12
$3 \cdot 2.75 \cdot 10^{-3}$	10
$4 \cdot 2.75 \cdot 10^{-3}$	9
$5 \cdot 2.75 \cdot 10^{-3}$	8
$6 \cdot 2.75 \cdot 10^{-3}$	7

actual μ in the experimental setup is for instance $4 \cdot 2.75 \cdot 10^{-3}$, the reference trajectory should at least begin at an initial value of $\omega_0 = 9$ Hz, to be able to define a lower-bound on μ. While the actual value of μ is unknown, the correct value of ω_0 during experiments should be found by trial-and-error.

To reduce the width of the confidence interval on μ, the values of $\dot{\omega}_{\text{low}}$ and $\dot{\omega}_{\text{high}}$ should be as close to each other as possible. Hereto, the minimum step-size of 1 Hz is taken as the step-size for the reference trajectory. This leads to the smallest discontinuous steps in $\dot{\omega}$ as possible. In section 4.1, the rotational velocity ω was increased quadratically to get a linear acceleration profile. Another solution in the variation of $\dot{\omega}$ during the profile is an inclined sine function:

$$\omega(t) = \omega_0 + \frac{\omega_e - \omega_0}{t_e}(t - t_0) - \frac{\omega_e - \omega_0}{2\pi}\sin(2\pi\frac{t - t_0}{t_e}),\ t_0 \leq t \leq t_e\,. \tag{4.8}$$

In (4.8), ω_0 and ω_e are the starting and ending rotational velocities respectively, while t_0 and t_e denote the start- and end-time of the profile. This signal starts and ends with zero acceleration $\dot{\omega}$ and has a maximum acceleration at $t = \frac{t_e - t_0}{2}$. While the reference trajectory should be a sequence of steps, it is chosen to approximate an inclined sine function by steps, where the first step starts at t_0. This signal will further be denoted as a staircase signal. An example of a staircase signal with $\omega_0 = -10$ Hz, $\omega_e = -15$ Hz, $t_0 = 0$ s and $t_e = 1$ s, is shown in figure 4.3. This staircase signal is used as $\dot{\theta}_{ref}$ in (4.5), whereas $\theta_{ref} = t\,\dot{\theta}_{ref}$. Some simulation results with this type of reference trajectory will be discussed in the next section.

4.2.3 Simulation results

Simulations are conducted for a value of the static friction coefficient of $2.75 \cdot 10^{-3}$. From table 4.1, it can be seen that the value of ω_0 should be -17 Hz to be able to define a lower-bound on μ. For an end reference velocity ω_e of -22 Hz and a begin- and end-time, t_0 and t_e, of 0 and 1 s, respectively, the resulting rotational velocity and acceleration of the ABU are shown in figures 4.4 and 4.5.

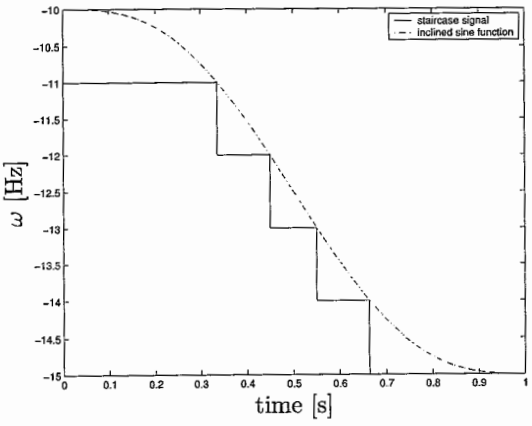

Figure 4.3: Step approximation of an inclined sine function.

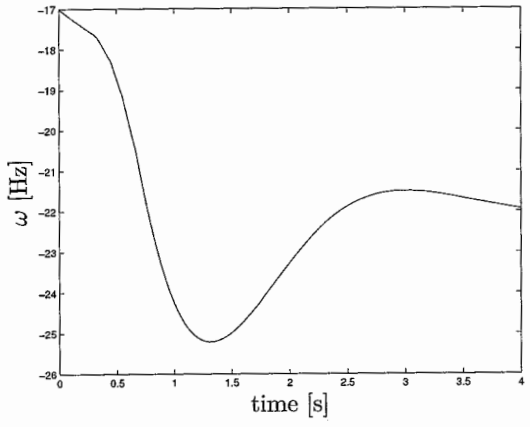

Figure 4.4: Rotational velocity ω of the ABU [Hz].

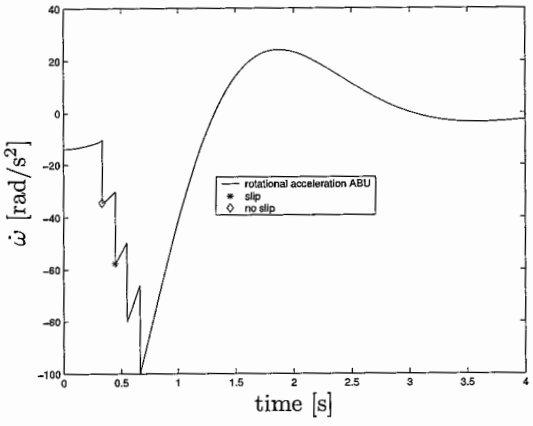

Figure 4.5: Rotational acceleration $\dot{\omega}$ of the ABU [rad/s^2].

As intended, a point can be identified for which no slip occurs (yielding $\dot{\omega}_{\text{low}}$) and for which the ball instantaneously starts slipping ($\dot{\omega}_{\text{high}}$). Moreover, in figure 4.5 five discontinuous steps can be distinguished, as the reference trajectory consists of five steps of 1 Hz. The slip-point can be identified from the results for β and $\dot{\beta}$ (see figures 4.6 and 4.7). Slip is detected when the relative angular velocity $\dot{\beta}$ becomes larger than a tolerance ϵ of 10^{-7} rad/s.

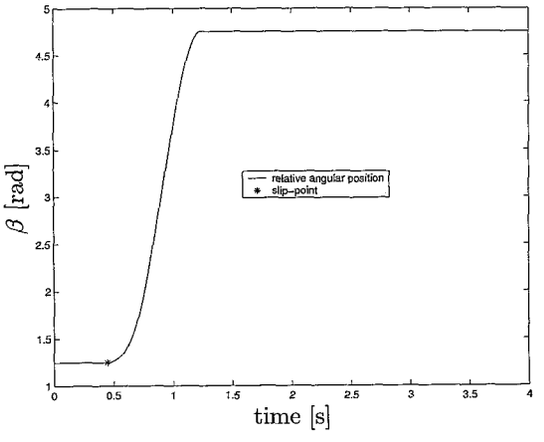

Figure 4.6: Relative angular position β [rad].

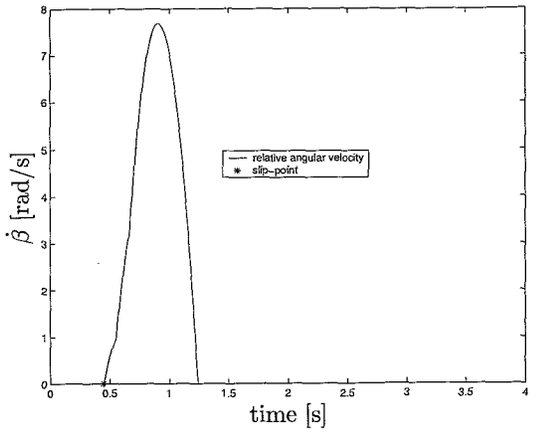

Figure 4.7: Relative angular velocity $\dot{\beta}$ [rad/s].

With the results for ω and $\dot{\omega}$ the lower- and upper-bound on μ is calculated using (4.7):

$$\begin{aligned} \mu_{\text{low}} &= 2.63 \cdot 10^{-3}, \\ \mu_{\text{high}} &= 4.14 \cdot 10^{-3}, \\ \mu_{\text{low}} &\leq \mu < \mu_{\text{high}}. \end{aligned} \tag{4.9}$$

The value of μ, used in this simulation ($2.75 \cdot 10^{-3}$), is indeed between both bounds. The accuracy of these bounds will not be regarded here. In chapter 5, an error-analysis with respect to the experiments is made.

Chapter 5

Static friction coefficient experiments

5.1 Experimental setup

For the static friction coefficient measurement, information on the angular velocity and acceleration of the ABU and the relative angular position of the ball is required. In the experimental setup, use is made of a high-speed camera to derive these measures. This camera is placed above the ABU and produces images that can be processed off-line (see figure 5.1). The table with ABU is rigidly

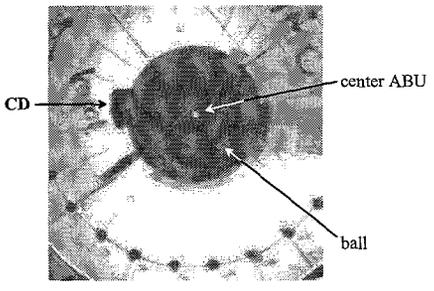

Figure 5.1: High-speed camera image.

attached to a granite block by two clamps, fixing all degrees of freedom but the rotational one. Furthermore, lighting is placed around the setup, which will be discussed separately in section 5.2 because of its importance. The total experimental setup with final lighting is shown in figure 5.2.

The image-processing returns x- and y-coordinates of markers. These markers are placed at the geometrical center of the ABU, at a certain point on the CD (remind point C from the derivation of the dynamic model of the ABU, chapter 3) and at the center of the ball. From these marker coordinates, angles θ and β are calculated. A thorough description of the markers, the image-processing and image-transfer can be found in appendix B.

5.2 Choice of lighting of the setup

To register the CD, ABU and ball, the camera needs a relatively large amount of light. Because diffuse light from the surrounding of the setup is not enough, additional lighting is applied. The lighting largely influences the results. During the experiments various methods of lighting are

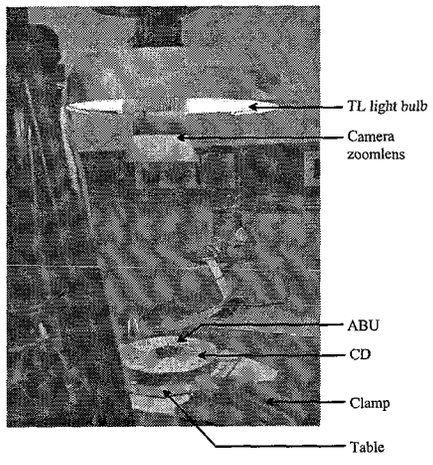

Figure 5.2: Experimental setup.

applied in order to improve the measurement results. Besides the final lighting setup, two other methods are tested. A brief description of these two methods is given below.

- *Direct lighting:* The first lighting-setup consists of a light-source directly aimed at the ABU. The brass ball is, however, so reflectant, that numerous lightened and darkened (shaded) regions can be distinguished on the camera image. This influences the determination of the midpoint of the ball. Various pieces of paper are put in front of the light-source to make the light more diffuse, without any succes.
- *Indirect lighting:* In this method, an umbrella-like shape is hung above the experimental setup with the aim to reflect the light of an upwards pointing light-source onto the ABU. To produce enough light, a stronger light-source (650 W) is aimed at the 'reflector' and two additional spots are put symmetrically around the ABU. It is decided to position the spots in such a way that two bright reflections appear on the ball. The reason for this will be explained later on. Both reflections are followed by a marker and the average of the two marker-positions is taken as the midpoint of the ball. At this moment, some results obtained with this lighting method will be presented to explain the final choice of lighting.

For a staircase input with $\omega_0 = -8$ Hz, $\omega_e = -18$ Hz, $t_0 = 0$ s and $t_e = 0.5$ s, the resulting relative angular position β is shown in figure 5.3. Furthermore, figure 5.4 shows the (absolute) rotational velocity ω of the ABU. As only the angular position θ can be measured, a differential scheme (central difference method) is used to calculate ω at time t:

$$\omega_t \approx \frac{\theta_{t+\Delta t} - \theta_{t-\Delta t}}{2\Delta t}. \tag{5.1}$$

Herein, Δt is determined by the sampling rate (4500 images per second) and equals 1/4500 s. Because of the relatively high sampling rate, the differential scheme returns quite a lot of noise. Decimation is applied to minimize this noise. From every ten samples of θ the average is taken and used in the differential scheme. The error introduced by applying this scheme will not be regarded here. A final error-analysis can be found in section 5.4. Figure 5.5 presents $\dot{\omega}$. The result is generated with the aid of a polynomial fit on ω. Differentiating the polynomial gives $\dot{\omega}$. This method is preferred above a differential scheme on ω or θ, because that introduces noise to such an extent that no usable results for $\dot{\omega}$ are obtained, even if decimation or filtering is applied. A disadvantage of the applied method is the unreliability of the polynomial fit near the beginning and end of the measurement series (here $t = 0$ and $t = 0.35$ s respectively). $\dot{\omega}$ can, however, be trusted in the rest of the region. Discontinuities in $\dot{\omega}$, as observed in the simulations of section

4.2, are not observed. An explanation for this can, at this moment, not be given.

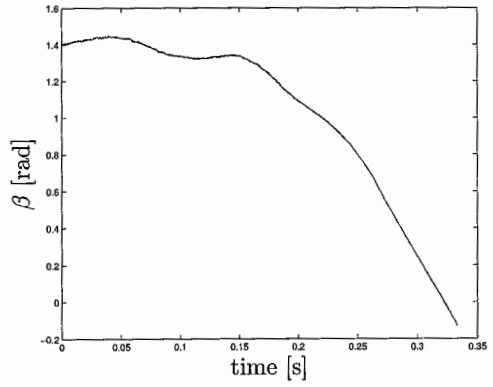

Figure 5.3: Relative angular position β [rad].

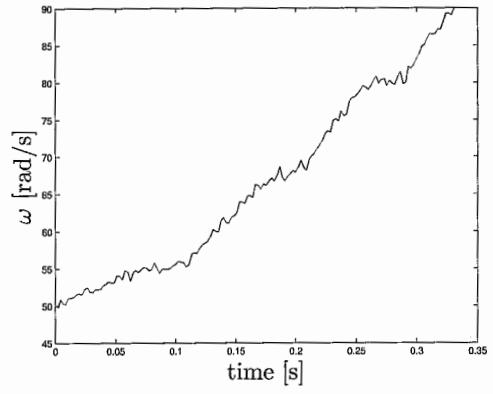

Figure 5.4: Angular velocity ω of the ABU [rad/s].

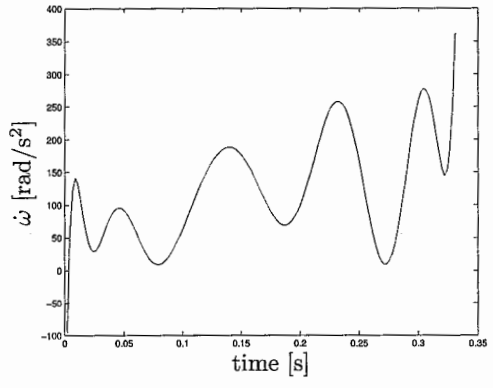

Figure 5.5: Angular acceleration $\dot{\omega}$ of the ABU [rad/s^2].

Apart from the fact that it is quite disputable whether the ball does not start to slip instantaneously during the first step of the profile, another feature in the result of β is striking. β does not change monotonically, but has a harmonic component with constant amplitude. One could carelessly conclude from this result that the ball apparently slips in both directions. The fluctuation in β can however *not* be caused by the varying value of $\dot{\omega}$. While ω is monotonically increasing during the regarded part of the profile, $\dot{\omega}$ is larger than zero in this region. If some value of $\dot{\omega}$ would be large enough to make the ball slip in a direction, an at least equally large negative value of $\dot{\omega}$ would be needed to make the ball slip in the other direction. Moreover, when operating the ABU at constant rotational velocity ($\dot{\omega} = 0$), the same harmonic disturbance is observed. The cause of this perturbation should therefore be sought in a different field.

It is observed that the frequency of the harmonic disturbance is close to the rotational velocity of the ABU. The fact that the lighting is asymmetric is therefore thought to cause a reproducible error in β. Although reproducible, it is very hard to compensate for, because of the changing value of ω. While the ball is depicted on relatively few pixels, a small change of position of the ball in combination with the asymmetric lighting results in a considerable change of brightness of these pixels, directly influencing the determination of the marker position. A larger zoom-factor could reduce the perturbation in β. The camera is, however, placed as close to the ABU as possible, so a maximum zoom-factor is already obtained and can not be enlarged any further. The reason for the applied lighting (resulting in two bright spots on the ball) is that the amplitude of the harmonic disturbance and the noise on β is reduced compared to previous measurements.

Besides a larger zoom-factor, a more symmetric lighting is beneficial to the reduction of the perturbation on β. Hereto, a final lighting-setup is constructed. A circular shaped TL-light bulb is placed around the lens of the camera (see figure 5.2). TL-light also has the advantage that it generates more diffuse light than ordinary spots.

5.3 Experimental results with final lighting setup

Twelve experiments are conducted with the final lighting setup. A staircase input with $\omega_0 = -9$ Hz, $\omega_e = -19$ Hz, $t_0 = 0$ s and $t_e = 0.5$ s, is used in all these experiments. During the measurements some additional advantages of the lighting setup are encountered. Apart from an easier image-processing, due to a better contrast between markers and the rest of the image, a reduction of the harmonic disturbance on β, as mentioned in section 5.2, is established. Although still present, the amplitude of the perturbation on β is reduced by a factor two. Figure 5.6 shows an example of the result of β, obtained during one of the experiments.

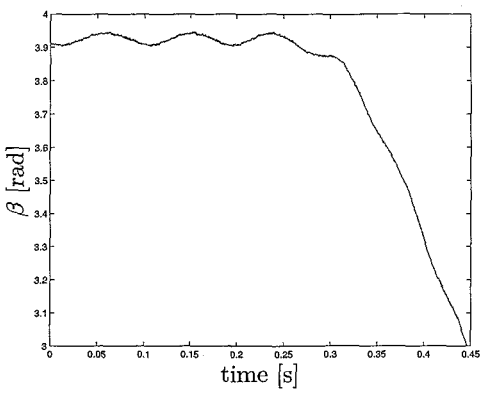

Figure 5.6: Relative angular position β [rad].

Figures 5.7 and 5.8 respectively present the (absolute) rotational velocity and acceleration of the ABU for that same measurement. Similar to the results discussed in section 5.2, $\dot{\omega}$ is calculated using a polynomial fit on ω. This causes inaccurate results for $\dot{\omega}$ between $t = 0$ and $t = 0.05$ s. In the rest of the depicted region the polynomial fit can be trusted.

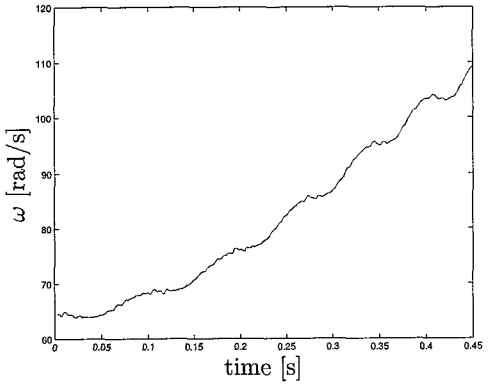

Figure 5.7: Angular velocity ω of the ABU [rad/s].

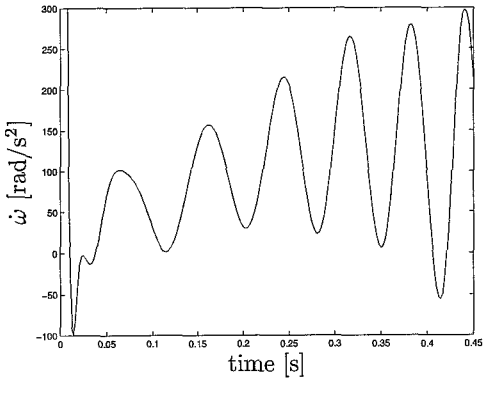

Figure 5.8: Angular acceleration $\dot{\omega}$ of the ABU [rad/s^2].

In the simulation results (section 4.2) bounding-values of μ were calculated (i.e. μ_{low} and μ_{high}). The required values of $\dot{\omega}$ followed from the discontinuous steps, where one of the steps caused slip instantly. In the experimental results, $\dot{\omega}$ is continuous and the slip-point can not be distinguished as clearly, so a different approach is needed in calculating the bounds on μ.

From figure 5.6 only a region of the time t can be given where slip occurs; $t_{\text{slip}} \in [0.10 \quad 0.33]$ s. In this region ω is monotonically increasing. In figure 5.8, there are a number of times in this region on which $\dot{\omega}$ reaches a maximum value. These times will be called as follows:

$t_1 = 0.160$ s,
$t_2 = 0.245$ s,
$t_3 = 0.315$ s.

For t_1 the ball is stated to be in stick. This can be concluded from the fact that β has not decreased significantly during $0 \leq t \leq t_1$, disregarding the harmonic disturbance. For t_3 the opposite can

be stated; the ball is clearly slipping. This means that somewhere between t_1 and t_3 the static friction force has reached its maximum value and the ball has started to slip. The state of the ball at t_2 can however not be confidently determined. ***Suppose*** that for every t the ball is in stick and $\dot{\beta} = \ddot{\beta} = 0$, then the static friction coefficient μ can be calculated from:

$$F_w = -\frac{\{ml^2 - \frac{2l}{d}J\}\dot{\omega}}{l}, \tag{5.3a}$$

$$F_N = ml\omega^2, \tag{5.3b}$$

$$\mu = \frac{|F_w|}{F_N}. \tag{5.3c}$$

The absolute value of F_w is once again taken because of the influence of the sign of $\dot{\beta}$ ($F_w \in \mu F_N \text{Sign}(\dot{\beta})$) as explained in section 4.1. Figure 5.9 shows the result when this principle is applied, where the polynomial fit on ω causes inaccurate results for μ between $t = 0$ and $t = 0.05$ s. Because of the monotonically increasing ω (and thus normal force), the maxima of μ correspond to maxima in $\dot{\omega}$. It was already stated that the ball is in stick at t_1, so (5.3a) to (5.3c) are valid and

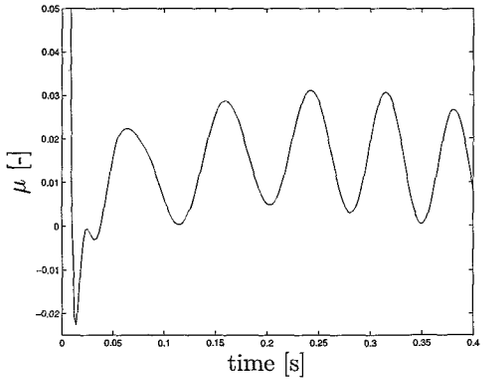

Figure 5.9: Static friction coefficient μ [-].

the value of μ in t_1 (μ_1) is correctly calculated (apart from an error introduced by errors in ω and $\dot{\omega}$, see section 5.4). This enables the determination of a lower-bound on μ of 0.0286. Regarding the values of μ at t_2 and t_3 it can be seen that μ_2 is larger than μ_3. From this finding an upper-bound on μ can be established.

If the ball would be in stick at t_2 it would remain in stick as long as $\dot{\omega}$ is decreasing. This is caused by the monotonically increasing ω and normal force. As it is unlikely that the static friction coefficient decreases for increasing normal force, it is obvious that $\dot{\omega}$ should at least become larger than its value at t_2 to possibly make the ball slip. Slip can only be induced at a point where ω and $\dot{\omega}$ reach such values that $\mu > \mu_2$. As there are no such points in figure 5.9, the only possible conclusion can be that the ball is already slipping in point t_2. The value μ_2 is thus an upper-bound on the static friction coefficient. For the considered experiment this results in the following confidence interval:

$$\mu \in \begin{bmatrix} 0.0286 & 0.0312 \end{bmatrix}.$$

The same procedure can be applied to all other experiments, resulting in twelve intervals on the static friction coefficient. In practice, friction is not a fixed quantity, so lower- and upper-bound are never the same. In some cases the lower-bound found in one experiment exceeds the upper-bound from another experiment! Factors like a particle of dust in the groove, the unroundness of the ball and the surface roughness (see figure 5.10) can influence the friction measurements.

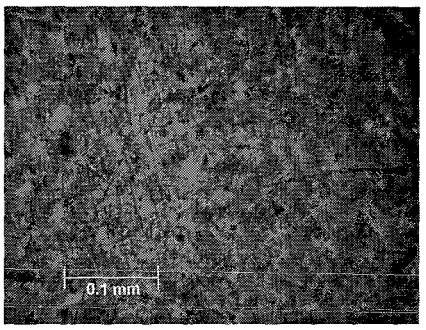

Figure 5.10: Microscopic view of the brass ball.

Despite all that, the bounds show large resemblance. The histogram in figure 5.11 presents the number of intervals in which a certain value of μ lies ($\mu_{\text{low}} \leq \mu \leq \mu_{\text{high}}$). A value of μ equal to 0.03 is for instance encountered in seven out of twelve intervals. From figure 5.11 a *total* confidence interval on μ of $[0.024 \quad 0.035]$ is identified. Because the calculated values of μ are not exact, an error analysis will be given in the next section.

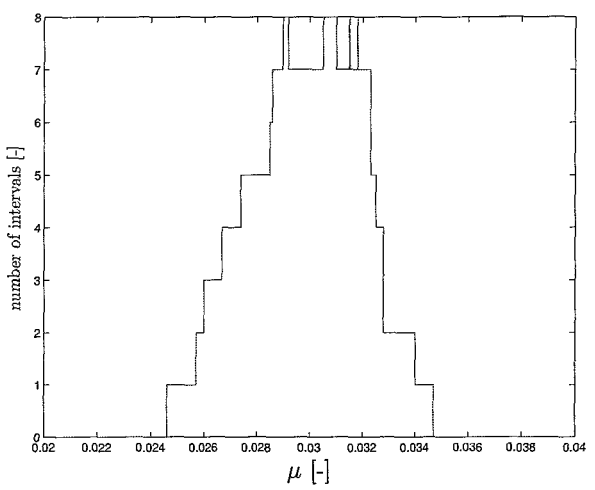

Figure 5.11: Histogram of μ and the number of intervals for which applies $\mu_{\text{low}} \leq \mu \leq \mu_{\text{high}}$.

5.4 Error analysis

There are a number of points that induce an error in the determination of the (bounds of the) static friction coefficient:

- *Image deformation:* Every camera slightly deforms an image. A perfect rectangle (straight edges exactly perpendicular to each other) will not be depicted perfectly on the image, but is distorted by the lens. This error is believed to be negligible small.

- *Image-processing:* The determination of the position of a marker introduces an error in the determination of the angles θ and β. An inaccuracy of 0.023 rad was found in [1].

- *Calculation of ω:* The differential scheme on θ (5.1) is accurate for linear and second-order functions in θ. For higher-order functions the error O equals:

$$O(\dot{\theta}) = -\frac{\dddot{\theta}}{6}\Delta t^2 + \text{ H.O.T.},$$

  where H.O.T. denote all uneven terms with order larger than three.

- *Reconstruction of $\dot{\omega}$:* The polynomial fit on ω is only an approximation of its true behaviour. When the derivative is taken also an error in $\dot{\omega}$ is introduced.

Unfortunately, it is very difficult to quantify the listed errors. Therefore, a 'calculated guess', following from evaluation of all measurements, of the errors in both ω and $\dot{\omega}$ is taken. ω and $\dot{\omega}$ are perturbed with an error ϵ_ω and $\epsilon_{\dot{\omega}}$, respectively:

$$\tilde{\omega} = \omega(1+\epsilon_\omega)\,, \tag{5.4a}$$

$$\tilde{\dot{\omega}} = \dot{\omega}(1+\epsilon_{\dot{\omega}})\,. \tag{5.4b}$$

The disturbed values of ω and $\dot{\omega}$ affect the calculated friction and normal force:

$$\tilde{F}_w = F_w(1+\epsilon_{\dot{\omega}})\,, \tag{5.5a}$$

$$\tilde{F}_N = F_N(1+\epsilon_\omega)^2\,. \tag{5.5b}$$

The perturbed value of the static friction coefficient ($\tilde{\mu}$) follows from (5.6):

$$\tilde{\mu} = \mu\left(\frac{1+\epsilon_{\dot{\omega}}}{(1+\epsilon_\omega)^2}\right) = \mu(1+\epsilon_\mu)\,. \tag{5.6}$$

When an error of 3% in ω and 5% in $\dot{\omega}$ is taken, the maximum error in μ equals 11.6%. Whereas [1] and [3] were only able to give an order estimate of μ, this research is able to define a confidence interval. Despite the relatively large error on the bounds, this forms a satisfactory result.

Chapter 6

Conclusions and recommendations

A friction measurement is designed and performed in order to identify the static friction level of an Automatic Balancing Unit with dry friction. Hereto, a dynamic model of the ABU, containing one ball and rigidly attached to the world, is derived. To model the friction between ball and the rim of the ABU, a set-valued Coulomb friction model is used. After numerical implementation in the software program MATLAB, simulations are conducted with both prescribed ABU motion and with practical restrictions to this motion. The first type of simulations show that the static friction coefficient can be determined accurately.

The restrictions of the ABU motion are imposed by the control and reference trajectory of the angular velocity in the experimental setup. Using an experiment, control parameters are identified and the control action is implemented in the ABU model. On simulation level, these restrictions result in discontinuous behaviour of the angular acceleration of the ABU, implying that only the determination of a confidence interval on the static friction coefficient is possible. Furthermore, a reference trajectory of the angular velocity of the ABU is generated to be used in experiments. Hereto, a sequence of steps of 1 Hz is used to approximate an inclined sine function.

In the experiments, a high-speed camera is used to generate images of the ABU and ball. After processing, relative angular position of the ball and angular velocity and acceleration of the ABU are obtained. Lighting of the experimental setup proves to have large influence on these measurements. The finally obtained lighting-setup is used in twelve experiments. In contrast to the simulations, the angular acceleration does not show discontinuities. A reason for this is, at this moment, not known. As a result of a harmonic disturbance on the relative angular position of the ball, the slip-point can not be distinguished clearly, so only a confidence intervals on the static friction coefficient is found. All obtained intervals are close to each other and show that the static friction coefficient is an order of magnitude larger than found in [1] and [3]. Whereas [1] and [3] only gave rough estimates of the static friction coefficient, this research has resulted in a relatively narrow confidence interval and small inaccuracy of the bounds.

For future research, dependency of the static friction coefficient on the normal force should be investigated. Reduction of the interval on the static friction coefficient and the inaccuracy of the bounds is necessary in such research. For this purpose, a precise detection of the slip-point is needed in combination with more accurate information on the angular velocity and acceleration of the ABU. Hereto, it should be possible to prescribe the motion of the ABU. A new controller, connectable to a laptop, that is capable of tracking a prescribed reference trajectory is strongly recommended. The value of the angular acceleration for which the ball starts to slip could then be investigated more accurately.

Moreover, improvement of the measurement of the angular positions of ball and ABU is necessary. It is desirable to use a high-speed camera that can be zoomed in more at the ABU. Further

improvement of the lighting setup and image-processing is also necessary. More attention should be paid at the reduction of the inaccuracy of the measurements. To be able to perform more measurements, a decrease of the measurement time is a must, since it forms a too large restriction at this moment.

Apart from the static friction level, effort should be put in finding the dynamic friction level, because this affects the stability of the equilibrium sets of the ball(s). Measurement or reconstruction of the relative angular velocity and acceleration of the ball is required for this.

Bibliography

[1] Heuvel, M.N. van den (2002), *Modeling and Analysis of an Automatic Balancing Unit with Dry Friction*, Eindhoven: Eindhoven University of Technology, Department of Mechanical Engineering, Dynamics and Control section. DCT-report 2002-67. M.Sc.-thesis.

[2] Leine, R.I. (2000), *Bifurcations in Discontinuous Mechanical Systems of Filippov-type*, Eindhoven: Eindhoven University of Technology, Department of Mechanical Engineering. Ph.D.-thesis.

[3] Koevoets, A.H. (2001), *Dynamics of an Automatic Dry Ball Balancer applied to a Disk System*, Eindhoven: Eindhoven University of Technology, Department of Mechanical Engineering, Dynamics and Control section. DCT-report 2001-28. M.Sc.-thesis.

[4] Wouw, N. van de (2001), *Multibody Dynamics*, Eindhoven: Eindhoven University of Technology, Department of Mechanical Engineering. Lecture Notes.

[5] *Readme.txt*, Readme file giving detailed information about the hard- and software of the ABU control unit and steering program MOT4.EXE.

[6] Landheer, D., Gee, A.W.J. de (1996), *Dynamische Contactverschijnselen*, Eindhoven: Eindhoven University of Technology. Lecture Notes, pp. 160-171.

[7] Kraker, A. de (2000), *A Numerical-Experimental Approach in Structural Dynamics*, Eindhoven: Eindhoven University of Technology, Department of Mechanical Engineering. Lecture Notes.

Appendix A

Derivation of the equations of motion

A.1 Elaboration of the kinematics

The kinematics introduced in section 3.2 will first be elaborated. The kinematics are expressed in

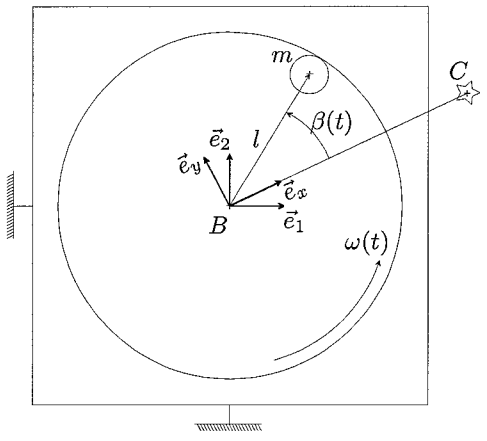

Figure A.1: Kinematics of the ABU model.

the generalized coordinates $\underline{q} = \begin{bmatrix}\beta(t) & l\end{bmatrix}^T$, see figure A.1. This gives the following position vector of the center of gravity of the ball:

$$\vec{r}_{A_m} = \begin{bmatrix} l\cos\beta(t) & l\sin\beta(t) \end{bmatrix} \begin{bmatrix} \vec{e}_x \\ \vec{e}_y \end{bmatrix}, \tag{A.1}$$

with:

$$\begin{bmatrix} \vec{e}_x \\ \vec{e}_y \end{bmatrix} = \begin{bmatrix} \cos\theta(t) & \sin\theta(t) \\ -\sin\theta(t) & \cos\theta(t) \end{bmatrix} \begin{bmatrix} \vec{e}_1 \\ \vec{e}_2 \end{bmatrix}, \tag{A.2}$$

where:

$$\theta(t) = \int_0^t \omega(\tau)d\tau\,,\ \theta(0) = 0\,. \tag{A.3}$$

Equation (A.1) can be rewritten as:

$$\vec{r}_{A_m} = \begin{bmatrix} l\cos\beta\cos\theta - l\sin\beta\sin\theta & l\cos\beta\sin\theta + l\sin\beta\cos\theta \end{bmatrix} \begin{bmatrix} \vec{e}_1 \\ \vec{e}_2 \end{bmatrix} . \tag{A.4}$$

Herein, the dependency of the coordinates on time is omitted. When the time-derivative of (A.4) is taken, $\dot{\vec{r}}_{A_m}$ can be derived:

$$\dot{\vec{r}}_{A_m} = \begin{bmatrix} -\dot{\beta}l\sin\beta\cos\theta - \dot{\theta}l\cos\beta\sin\theta - \dot{\beta}l\cos\beta\sin\theta - \dot{\theta}l\sin\beta\cos\theta + \dot{l}\cos\beta\cos\theta - \dot{l}\sin\beta\sin\theta \\ -\dot{\beta}l\sin\beta\sin\theta + \dot{\theta}l\cos\beta\cos\theta + \dot{\beta}l\cos\beta\cos\theta - \dot{\theta}l\sin\beta\sin\theta + \dot{l}\cos\beta\sin\theta + \dot{l}\sin\beta\cos\theta \end{bmatrix}^T \begin{bmatrix} \vec{e}_1 \\ \vec{e}_2 \end{bmatrix} . \tag{A.5}$$

The rotational velocity of the ball (ω_{ball}) can be expressed in $\dot{\beta}$ and ω. Due to the kinematic

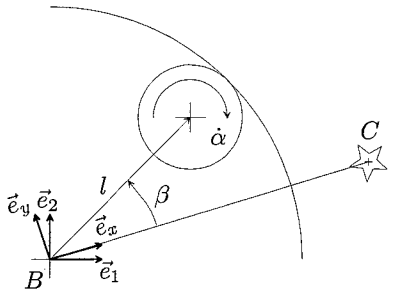

Figure A.2: Relationship between $\dot{\alpha}$, $\dot{\beta}$ and ω due to the kinematic constraint.

constraint, implying that no slip occurs in the contacting surfaces, the following relation holds (see figure A.2):

$$-\frac{d}{2}\dot{\alpha} + (l + \frac{d}{2})\dot{\beta} = 0 \implies \dot{\alpha} = (\frac{2l}{d} + 1)\dot{\beta} . \tag{A.6}$$

The symbol d is used to denote the diameter of the ball. Hence the circular disk of the ABU has a rotational velocity, the rotational velocity of the ball can be derived:

$$\omega_{\text{ball}} = -\dot{\alpha} + \dot{\beta} + \omega = -\frac{2l}{d}\dot{\beta} + \omega . \tag{A.7}$$

Or, in vector notation:

$$\vec{\omega}_{\text{ball}} = \{-\frac{2l}{d}\dot{\beta} + \omega\}\vec{e}_z , \tag{A.8}$$

with $\vec{e}_z$ the vector following from both right-handed coordinate systems ($\vec{e}_1$,$\vec{e}_2$) and ($\vec{e}_x$,$\vec{e}_y$); $\vec{e}_z = \vec{e}_1 \times \vec{e}_2 = \vec{e}_x \times \vec{e}_y$.

A.2 Kinetic and potential energy

With the elaborated kinematics, the kinetic energy of the system can be given by:

$$T = \frac{1}{2}m\dot{\vec{r}}_{A_m} \cdot \dot{\vec{r}}_{A_m} + \frac{1}{2}J\vec{\omega}_{\text{ball}} \cdot \vec{\omega}_{\text{ball}} . \tag{A.9}$$

While the ball has negligible influence on the motion of the ABU it can be regarded decoupled from the rest of the system (see section 4.2.1). Using (A.3), (A.5) and (A.8) the kinetic energy T becomes:

$$T = \frac{1}{2}m\{\dot{\beta}^2l^2 + \dot{\theta}^2l^2 + 2\dot{\theta}\dot{\beta}l^2 + \dot{l}^2\} + \frac{1}{2}J\{\frac{4l^2}{d^2}\dot{\beta}^2 - \frac{4l}{d}\dot{\theta}\dot{\beta} + \dot{\theta}^2\} . \tag{A.10}$$

The potential energy V consists of gravitational and elasticity terms. Since the ABU is placed in a horizontal plane and is assumed to only have motions in this plane, there are no gravitational terms. Moreover, the ABU is rigidly attached to inertial space, resulting in zero elasticity terms. Therefore, the potential energy V obeys:

$$V = \text{constant}. \tag{A.11}$$

A.3 Non-conservative forces

Because of the rigid attachment of the ABU to the fixed world, there are no damping terms. As a result, the non-conservative forces only consist of the friction force acting on the ball. This force is defined to act on the ball in its center of gravity, tangential to the contact surface [6] (see figure A.3). The column of non-conservative forces $\underline{Q}^{\text{nc}}$ can be derived using (A.12) [4]:

$$\underline{Q}^{\text{nc}} = \left(\frac{\partial \vec{r}}{\partial \underline{q}}\right)^T \cdot \vec{F}^{\text{nc}}, \tag{A.12}$$

with:

$\vec{r}$	absolute position vector of the point in which the non-conservative force is exerted;
$\underline{q}$	column of generalized coordinates;
$\vec{F}^{\text{nc}}$	non-conservative force vector.

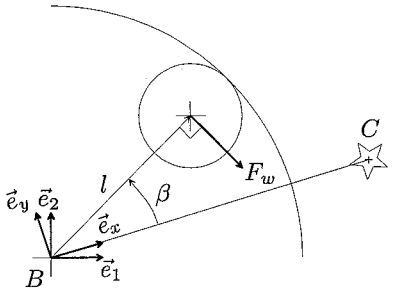

Figure A.3: Schematic representation of the non-conservative force.

Using figure A.3, the vectors $\vec{r}$ and $\vec{F}^{\text{nc}}$ can be expressed as:

$$\vec{r} = \begin{bmatrix} l\cos\beta & l\sin\beta \end{bmatrix} \begin{bmatrix} \vec{e}_x \\ \vec{e}_y \end{bmatrix}, \tag{A.13a}$$

$$\vec{F}^{\text{nc}} = F_w \begin{bmatrix} \sin\beta & -\cos\beta \end{bmatrix} \begin{bmatrix} \vec{e}_x \\ \vec{e}_y \end{bmatrix}, \tag{A.13b}$$

yielding:

$$\underline{Q}^{\text{nc}} = \begin{bmatrix} -lF_w \\ 0 \end{bmatrix}. \tag{A.14}$$

A.4 Normal force

The normal force ensures that the ball always remains in contact with the rim of the ABU. This constraint (l = constant) is written at acceleration level:

$$\underline{R}\ddot{\underline{q}} = 0\,. \tag{A.15}$$

Using $\ddot{l} = 0$, the following expression for $\underline{R}$ can be derived:

$$\underline{R} = \begin{bmatrix} 0 & -1 \end{bmatrix}\,. \tag{A.16}$$

The minus sign in $\underline{R}$ is added because positive values of F_N are defined as compressive forces. The column of constraint forces can be calculated using $\underline{Q}^{constr} = \underline{R}^T\underline{\lambda}$, with $\underline{\lambda} = F_N$.

A.5 Equations of motion

Lagrange's equations of motion for systems with constraints can be written as:

$$\frac{d}{dt}(T_{,\underline{\dot{q}}}) - T_{,\underline{q}} + V_{,\underline{q}} = (\underline{Q}^{\mathrm{nc}})^T + (\underline{R}^T\underline{\lambda})^T\,. \tag{A.17}$$

The result of (A.17) can be rewritten as:

$$\underline{M}(\underline{q})\ddot{\underline{q}} - \underline{h}(\underline{q},\dot{\underline{q}}) + \underline{S}\,\underline{\lambda} = \underline{R}^T\underline{\lambda}\,. \tag{A.18}$$

The expressions for $\underline{M}(\underline{q})$ and $\underline{h}(\underline{q},\dot{\underline{q}})$ are the following:

$$\underline{M}(\underline{q}) = \begin{bmatrix} ml^2 + J(\frac{2l}{d})^2 & 0 \\ 0 & m \end{bmatrix}\,, \tag{A.19}$$

$$\underline{h}(\underline{q},\dot{\underline{q}}) = \begin{bmatrix} h_\beta & h_l \end{bmatrix}^T\,, \tag{A.20}$$

with:

$$\begin{aligned} h_\beta &= -\{ml^2 - J(\tfrac{2l}{d})\}\ddot{\theta}\,, \\ h_l &= -\{J\tfrac{2}{d}\dot{\theta}\dot{\beta} - ml(\dot{\beta}+\dot{\theta})^2 - J(\tfrac{4l}{d^2})\dot{\beta}^2\}\,. \end{aligned}$$

The state of the ball (*Stick*, *Slip* or *Transition*) determines the expressions for $\underline{\lambda}$, $\underline{R}$ and $\underline{S}$. The possible configurations will be discussed in the next section.

A.6 State configurations

A.6.1 Slip

In the case where the ball is in slip, the friction force equals the static level and can thus be calculated using $F_w \in \mu F_N \mathrm{Sign}(\dot{\beta})$. There remains only one constraint force, namely F_N. $\underline{\lambda}$, $\underline{R}$ and $\underline{S}$ are equal to:

$$\underline{R} = \begin{bmatrix} 0 & -1 \end{bmatrix}\,, \tag{A.21a}$$

$$\underline{S} \in \begin{bmatrix} \mu l \mathrm{Sign}(\dot{\beta}) \\ 0 \end{bmatrix}\,, \tag{A.21b}$$

$$\underline{\lambda} = F_N\,. \tag{A.21c}$$

A.6.2 Stick

Stick is defined as the state where $\dot{\beta} = 0$ and $\ddot{\beta} = 0$. The friction force is calculated as a constraint force, counteracting the resultant of all other external forces. This has the following implications for $\underline{\lambda}$, $\underline{R}$ and $\underline{S}$:

$$\underline{R} = \begin{bmatrix} -l & 0 \\ 0 & -1 \end{bmatrix}, \tag{A.22a}$$

$$\underline{S} = \begin{bmatrix} 0 & 0 \\ 0 & 0 \end{bmatrix}, \tag{A.22b}$$

$$\underline{\lambda} = \begin{bmatrix} F_w \\ F_N \end{bmatrix}. \tag{A.22c}$$

A.6.3 Transition

At some moment $\ddot{\beta} \neq 0$ and $\dot{\beta} = 0$. To numerically tackle this situation, the transition state is defined. Depending on the sign of $\ddot{\beta}$, there are two possible solutions, denoted by $\oplus$ and $\ominus$. The friction force equals the static friction level.

$$\underline{R} = \begin{bmatrix} 0 & -1 \end{bmatrix}, \tag{A.23a}$$

$$\underline{S}_{\oplus} = \begin{bmatrix} \mu l \\ 0 \end{bmatrix}, \tag{A.23b}$$

$$\underline{S}_{\ominus} = \begin{bmatrix} -\mu l \\ 0 \end{bmatrix}, \tag{A.23c}$$

$$\underline{\lambda} = F_N. \tag{A.23d}$$

Appendix B

Image-processing and -transfer

Three markers are used to measure the angles θ and β from the high-speed camera images. Every image is built up by pixels. In this case, one image consists of 256·256 pixels. The high-speed camera is capable of recording 4500 images per second. Due to the limited capacity of the memory of the camera, only 3072 frames are stored, corresponding to a measurement time of approximately 0.68 s. After recording, the images are downloaded to the computer that is coupled to the camera. This proves to be very time-consuming. The time required to download one image is approximately 2.5 to 3 s. For a series of 2500 images this takes more than two hours! Unfortunately this download-time can not be changed as it is determined by the camera and its interface.

The image-processing is performed with MATLAB. The images do therefore need to be transferred to the laptop. Because every picture has a size of 67 kB, a measurement series can rapidly exceed 150 Mb. To speed up the image-transfer, an ftp-account is created on a local network. This minimizes the total transfer-time of one measurement to approximately 25 minutes. No other solutions are found to reduce this even further.

The image-processing itself is relatively fast. Use is made of an already existing MATLAB routine. First, the user is asked to give the number of markers that need to be traced. After that, an initial starting point in the vicinity of each marker is given. Furthermore, a window-size is chosen. This window is put symmetrically around the initial starting point. In this window, a number of contour lines are made between a certain upper- and lower-bound. These bounds are determined as a percentage of the difference between the highest and lowest pixel value in the window (brightest and darkest pixel, respectively). Using a circle-fit method [7], the center of the contour lines is determined (see figure B.1). The x- and y-coordinate of the center of each marker

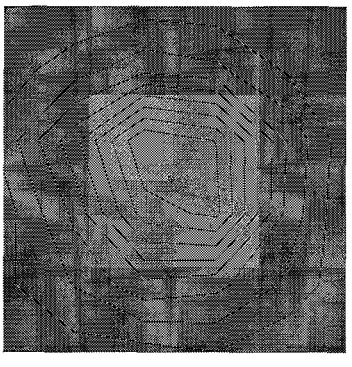

Figure B.1: Example of a high-speed image with contour-lines and calculated center (⊗), zoomed in at the ball.

is placed into a matrix. These centers are used as the starting points of the windows for the next image. After processing, one matrix with x- and one with y-coordinates is returned. Each matrix has dimensions (number of images * number of markers). Using the measurements of the positions of the markers on the CD and ball relatively to the marker on the center of the ABU, angles θ and β can be calculated. The movement of the marker on the center of the ABU during the measurement series is negligibly small.

The total measurement and processing-time is very large (approximately 3 to 4 hours). This puts a large constraint on the number of experiments that can be performed during one day. Experiments should, therefore, be planned in advance with utmost care, so no valuable measurement-time is lost.